PCCP

Accelerated lithium-ion diffusion via a ligand 'hopping' mechanism in lithium enriched solvate ionic liquids

Journal:	*Physical Chemistry Chemical Physics*
Manuscript ID	CP-ART-09-2023-004666
Article Type:	Paper
Date Submitted by the Author:	26-Sep-2023
Complete List of Authors:	Harte, Timothy; Deakin University, Institute for Frontier Materials Dharmasiri, Bhagya; Deakin University, Institute for Frontier Materials DOBHAL, GARIMA SUMIT; Deakin University, Institute of Frontier Materials Walsh, Tiffany; Deakin University, Institute for Frontier Materials Henderson, Luke; Deakin University, Institute for frontier materials

ARTICLE

Accelerated lithium-ion diffusion via a ligand 'hopping' mechanism in lithium enriched solvate ionic liquids.

Timothy Harte,[a] Bhagya Dharmasiri,*[a] Garima S. Dobhal,[a] Tiffany R. Walsh,*[a] and Luke C. Henderson*[a]

Received 00th January 20xx,
Accepted 00th January 20xx

DOI: 10.1039/x0xx00000x

Solvate ionic liquids (SILs), equimolar amounts of lithium salts and polyether glymes, are well studied highly customisable "designer solvents". Herein the physical, thermal and ion mobility properties of SILs with increased LiTFSI (LiTFSA) concentration, with ligand 1:>1 LiTFSI stoichiometric ratios, are presented. It was found that between 60-80 °C, the lithium cation diffuses up to 4 times faster than the corresponding anion or ligand (glyme). These systems varied from viscous liquids to self-supporting gels, though were found to thin exponentially when heated to mild temperatures (50-60 °C). They were also found to be thermally stable, up to 200 °C, well in excess of normal operating temperatures. Ion mobility, assessed under an electric potential via ionic conductivity, showed the benefit of SIL optimisation for attaining greater concentrations of Li^+ cations to store charge during supercapacitor charging and discharging. Molecular dynamics simulations interrogate the mechanism of enhanced diffusion at high temperatures, revealing a lithium hopping mechanism that implicates the glyme in bridging two lithiums through changes in the denticity.

Introduction

Ionic liquids (ILs) have numerous applications in various fields, including materials science, chemistry, and biology.[1] This is largely due to their tailorability from limitless constitutional variations,[2] ability to act as reaction media, electrolytes,[3] and enhancing biological activity in pharmaceuticals.[4]

They are desirable for their non-flammability, wide electrochemical potential window, negligible vapour pressure, high ionic conductivity, high chemical stability and solubilising power.[5, 6] ILs are of particular interest as electrolytes in lithium ion batteries (LIB),[7, 8] as they obviate risks associated with traditional LIB electrolytes ($LiPF_6$ and organic solvents) which are flammable and degrade above 60 °C in the presence of water.[9] This temperature (60 °C) is lower than typical electric vehicle operating temperatures without active or passive cooling.[10] ILs are alternatives to traditional electrolytes, capable of routine operation at relevant temperatures, making them potential candidates for application in uncooled structural supercapacitors in electric vehicles.

Solvate ionic liquids (SILs) are one of four groups of ILs,[11] and were first identified as a distinct IL in their own right by Tamura *et al*. in 2010.[12] SILs have three components, a salt consisting of a cation and anion, and a ligand molecule (usually an oligoether) that is coordinated to one of these ions. SILs typically exist by chelating a hard cation, in this case lithium, thereby diffusing and 'softening' the cationic charge over multiple atoms (**Fig. 1**, **a** & **b**).[11] SILs have been used as electrolytes in LIBs,[13-16] as a sizing agent for carbon fibre in structural composites,[17] as reaction media,[1, 18] and in bi-continuous electrolyte systems in structural supercapacitors.[19] SILs can be thought of as "designer solvents", as alteration of component ligands, cations & anions can be used to tune the physicochemical properties of the SIL.[20-22]

SILs used in this study were lithium bis(trifluoromethanesulfonyl)imide (LiTFSI, also called TFSA, bis(trifluoromethylsulfonil)amide) dissolved in either triethylene glycol dimethyl ether (G3) or tetraethylene glycol dimethyl ether (G4) shown in **Fig. 1**.

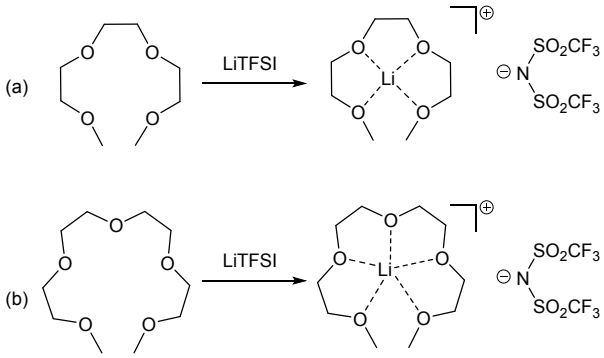

Fig. 1 Generalised reaction scheme and structures of G3 (a) and G4 (b).

A limitation of these SILs is their human and environmental toxicity, however this must be placed in context with the environmental pollution potential and toxicity posed by

[a] *Institute for Frontier Materials, Deakin University, Waurn Ponds, Victoria 3216, Australia*
** Corresponding authors. E-mail addresses: luke.henderson@deakin.edu.au (L.C. Henderson), tiffany.walsh@deakin.edu.au (T.R. Walsh). & k.dharmasiri@deakin.edu.au (B. Dharmasiri).*
† Electronic Supplementary Information (ESI) available: [Additional NMR, Rheological, Thermal analysis, MD simulation procedures, and electrochemical data are available]. See DOI: 10.1039/x0xx00000x

traditional LIB electrolytes ($LiPF_6$) and the application of G3 and G4 as comparatively lower toxicity solvents.[23-25]

Henderson *et al*. first characterised Li^+ salts chelation with G3/G4 ethereal solvents and Eyckens *et al*. with respect to Kamlet-Taft and Gutmann (Lewis Acid) acceptor properties.[1, 26, 27] Tong *et al.* investigated the effect of increasing Li^+ salt concentrations in imidazolium ionic liquids (e.g. [C2mim][TFSI]), experimentally and in conjunction with molecular dynamics simulations. Findings showed ILs had higher viscosity, density and lithium transference numbers (t_{Li}) with increasing LiTFSI concentration.[28] The effect on physical and electrical properties with increasing LiTFSI concentration in SIL systems, greater than 1:1, remains unexplored. At 1:1 ratios [Li-G3]TFSI and [Li-G4]TFSI fulfil the SIL criteria outlined by Mandai *et al*.,[29] and have properties consistent with ILs.[30] At higher Li salt concentrations [Li-G3]TFSI and [Li-G4]TFSI can be considered as concentrated lithium salts in solvent, lithium enriched SILs or quasi-SILs. With higher LiTFSI ratios, [Li-G3]TFSI and [Li-G4]TFSI can be considered, in effect, ILs as they maintain their physical properties of low vapor pressure, thermal stability, and high ionic conductivity.

G3/G4 Lewis base oligo-ether groups coordinate with the lithium cation, diffusing the charge of the ion and enabling the dissolution of LiTFSI. The influence of the ratio of ethereal solvent ether oxygens to Li cations was of theoretical interest, as G3 (of analogous carbon and oxygen number as 12-crown-4) is the ideal size for Li^+ chelation with four ether oxygen atoms per Li^+ cation.[31, 32] The SIL composed of 1:1 [Li-G4]TFSI is of interest as the lithium-to-oxygen ratio is 1:5, offering the potential to coordinate additional lithium cations.

Previous work by Dharmasiri *et al*. used 1:1 [Li-G3]TFSI, SIL:epoxy (7:3, w/w), in a resin encapsulated bi-continuous electrolyte system for structural carbon fibre (CF) supercapacitors.[19] High LiTFSI concentrations in [Li-G3]TFSI and [Li-G4]TFSI SILs can create conductive gels due to the increase in viscosity with increasing LiTFSI concentration.[20] High concentration SILs with increased LiTFSI may serve as a route to solid-state electrolytes, eliminating the need for encapsulation in bi-continuous resin systems, as done previously with other SILs.[33, 34]

The goal of studying these mixed systems being that when more ions are available for polarisation and migration during charging, the potential to increase the total charge stored in a capacitor also increases. Optimising electrolyte ion concentration could improve the performance of structural supercapacitors, as pseudocapacitance and EDLC are both affected by diffusion-controlled processes and EDL formation is influenced by ion concentration.[35-42]

As mentioned previously, increasing lithium concentration in SILs increases viscosity,[20] so the benefits of increased ion concentration during supercapacitor charging may come at a cost to reduced ion mobility in higher viscosity solutions. Ueno *et al*. previously investigated 1:1 G3:LiTFSI and G4:LiTFSI physical properties including ^7Li,^1H, and ^{19}F rates of self-diffusion at 30 °C, ionic conductivity and thermal properties.[43] Findings showed that [Li-G3]TFSI had a higher viscosity (169 mPa s) compared to [Li-G4]TFSI (81 mPa s). Conversely, [Li-G4]TFSI had a higher ionic conductivity than [Li-G3]TFSI at 1.6 $mScm^{-1}$ and 1.1 $mScm^{-1}$, respectively, as would be expected from their viscosity. The t_{Li} values for 1:1 G3:LiTFSI and G4:LiTFSI were 0.6 and 0.52, respectively, while the self-diffusion coefficients were D_{Li} 0.89, D_H 0.84 & D_F 0.57 for G3 and D_{Li} 1.31, D_H 1.29 & D_F 1.22 for G4 (all of the same magnitude, $x10^{-7}$ cm^2s^{-1}).[43]

Yoshida *et al*. has previously investigated sub-stoichiometric lithium salt ratios, increasing concentrations of ether solvents in a range from 400:1 to 1:1 (G3/G4:LiTFSI) and reported ^7Li,^1H, and ^{19}F rates of self-diffusion, viscosity and ionic conductivity at 30 °C.[20, 43] In that work, viscosity increased with increasing LiTFSI concentration, while ionic conductivity peaked, at ~ 3.7(G3) and 3.3(G4) $mScm^{-1}$, at approximately 4:1 G3/G4:LiTFSI and decreased to ~ 1.6(G3) and 1(G4) $mScm^{-1}$, values similar to 1:1 ratios reported by Ueno *et al*. Self-diffusion of ethereal solvents was ~60% faster than Li^+ & $TFSI^-$ for higher solvent ratios and approximately equal for 1:1 ratios.[20, 43]

Aguilera *et al.* examined the nano-structure of G4:LiTFSI across a range of concentrations, from dilute to equimolar, utilising small-angle X-ray scattering (SAXS) and Raman spectroscopy. The population of uncoordinated G4 was found to decrease with LiTFSI concentration increasing and even at equimolar ratios a population of uncoordinated G4 existed.[44] Previous G3/G4:LiTFSI molecular dynamics simulations by Jankowski *et al*. focused on reducing LiTFSI concentration from equimolar ratios.[45]

Herein, we address the current research gap on understanding physical, thermal, ion mobility and self-diffusion properties of lithium enriched G3/G4:LiTFSI. The glyme:LiTFSI stoichiometries examined here are 1:4 and 1:3.5, for G3, 1:1.75 and 1:1.25 for G4, and 1:3, 1:2.5, 1:2, 1:1.5 and 1:1 for G3 and G4, for context and comparison to literature values. We report the self-diffusion properties of ^7Li,^1H, and ^{19}F nuclei, and Li^+ transference numbers, present in G3/G4:LiTFSI samples over a temperature range, 20-80 °C, relevant to their application as electrolytes in energy storage applications.[10] To complement those data, ion mobility, thermal stability and thermal phase state are also presented to provide context on how these materials handle and can be processed.

Experimental Methods

Materials and Methods

All chemicals and solvents were purchased from Sigma-Aldrich Australia and used without further purification.

Sample nomenclature. SIL samples are named as G(Glyme)[3 or 4]-(Glyme:LiTFSI Molar ratio). For instance, G3-1:2 refers to a triglyme sample with a 1:2 molar ratio of glyme to LiTFSI.

Diffusion NMR measurements. Multinuclear (^7Li, 155.3 MHz; ^1H, 399.7 MHz; and ^{19}F, 376.1 MHz) NMR relaxation and diffusion measurements of SIL samples were performed at temperatures from 20-80 °C in increments of 10 °C for all samples and from 50-80 °C in increments of 5 °C for sample ratios between 1:1 and 1:2. Samples were allowed to

equilibrate for at least 5 minutes at each temperature after instrument temperature stability was reached.

A double stimulated echo Pulse Field Gradient (PFG) NMR pulse sequence, developed and previously used by Gunathilaka *et al*. 2022,[46] was used to reduce the effect of convection on the measurements. Decay data was fitted to a single exponential function using Bruker Topspin software v3.6.5. All measurements were conducted on a Bruker Ascend 300WB superconducting magnet connected to a Bruker Avance III NMR spectrometer system using BCU II & BCU 20 temperature regulation systems at a field strength of 7.05 T (70500 Gauss, v = 300 MHz).

The gradient pulse duration δ was fixed at 2.0 ms, and maximum gradient strength and diffusion observation time were optimised for each sample. For ^{1}H, maximum gradient strength was chosen between 3 and 27 Tm^{-1}, with diffusion observation time (Δ) between 25 and 110 ms. For ^{19}F, maximum gradient strength was chosen between 5 and 27 Tm^{-1}, with diffusion observation time (Δ) between 25 and 130 ms. For ^{7}Li, maximum gradient strength was chosen between 10 and 29.7 Tm^{-1}, with diffusion observation time (Δ) between 25 and 750 ms. Repetition time was 1.00 s for ^{1}H and ^{19}F nuclei and between 1.00 and 1.46 for ^{7}Li nuclei.

The standard deviation of diffusion coefficients for the samples between 1:1 and 1:2 for G3 and G4 were calculated by repeating measurements at 80 °C for the 3 nuclei. The calculated standard deviation is reported in Table S1 (ESI). For higher ratio samples, the standard deviation for G3 and G4 1:2 nuclei diffusion measurements was used as the variation was negligible in these samples.

Li^+ transference numbers (t_{Li}) were calculated by equation (1) below.

$$t_{Li} = \frac{D_{Li}}{D_{Li} + D_F} \quad (1)$$

where D_{Li} and D_F are the diffusion coefficients for Li^+ and F nuclei, respectively. The authors acknowledge that equation (1) does not account for dynamic ion correlations and cross-correlation effects.[47]

Rheology. Rheological experiments were conducted on a TA Instruments HR-1 Rheometer using parallel plate geometry, with disposable 25 mm diameter aluminium plates. A frequency of 1 Hz, strain of 0.01 (1%), 25 µm trim gap and 500 µm gap between plates (minimum sample volume of 245 µL) was used for all measurements. A flow temperature ramp experiment method, heating at 1 °C/min from 25 to 80 °C, was used to measure change in complex viscosity versus temperature.

Fitting of experimental viscosity data was performed using the Vogel-Fulcher-Tamman (VFT) equation (2) below.

$$\log_{10}\eta^* = A + \frac{B}{T - T_0} \quad (2)$$

where $\eta^*$is complex viscosity, A is η^*_0 (Pa·s), B and T_0 are constants.[20, 48] Complex viscosity (η^*) as opposed to viscosity (η) was measured as viscosity cannot be measured on parrel plate geometry rheometers. η^* differs from η by accounting for dynamic material behaviour under oscillatory shear. Unlike η, which measures resistance to steady flow, η^*assesses both elastic and viscous reactions to changing shear rates. η^* is used as an accurate measure of η in various published works.[49, 50]

Differential Scanning Calorimetry (DSC). DSC experiments were performed with a Netzsch Polyma DSC instrument. Samples were heated to 120 °C at 10 K/min, held isothermally for 5 min, to remove residual water, cooled to –70 °C at 10 K/min, held isothermally for 5 min and heated to 120 °C at 5 K/min. The final heating cycle was used for data analysis. T_g and T_m(°C) were taken as the midpoint of these transitions. T_L/$_L$ (°C) was taken as the midpoint of the liquid-liquid phase transition that occurs around room temperature.

Thermo-gravimetric analysis (TGA). TGA experiments were performed on a Netzsch TG 209 F1 Libra. Less viscous samples (G3/4 1:1 to 1:2) were heated to 120 °C at 20 K/min, held isothermally for 5 min, to remove residual water. More viscous samples (G3/4 1:2.5 to 1:4) were heated to 130 °C at 20 K/min, held isothermally for 10 min and cooled to 100 °C at 20 K/min. Samples were then heated to 600 °C at 10 K/min under N_2 atmosphere. Greater isothermal water removal drying time was applied in more viscous samples as the high viscosity of these sample inhibits drying. T_d (°C) was determined as the temperature at which a 5% mass loss occurred above 150 °C. This method was modified from literature, Ueno *et al*. 2012,[43] as the 5% mass loss > 150 °C was found to be more reliable with atmospheric exposure of ionic liquid samples occurring during TGA sample preparation.

Ionic Conductivity. Electrochemical impedance spectroscopy (EIS) experiments were performed with a Biologic SP300 Potentiostat Electrochemical station using Biologic EC-Lab v11.42 software in an air condition temperature-controlled room at 17.5 °C ±0.5 °C. The frequency was swept from between 100.000 mHz to 100.000 kHz with 10 points per decade and a sinus amplitude of 10.0 mV.

During EIS measurements, liquid samples of G3&G4-1:1 to 1:2 (1 mL) at room temperature (17.5 °C ±0.5 °C) were placed between two 0.55 mm copper plates in a 1x1x2 cm 3D printed plastic sample holder. Measurements were conducted in a two-electrode configuration. Ionic conductivity (δ) was calculated using equation (3) below.

$$\delta = \frac{d}{R_b S} \quad (3)$$

where d is the thickness of the electrolyte sample (the distance between the copper plates on the inside of the 3D printed sample holder), R_b is the bulk resistance of the sample and S is the surface area of the sample in contact with the electrodes.

Synthesis

Synthesis of SILs [Li-G3]TFSI and [Li-G4]TFSI drew on previously published reports for equimolar [Li-G3]TFSI and [Li-G4]TFSI synthesis.[49] LiTFSI and G3/G4 were combined at different molar ratios according to **Table 1** to form [Li-G3]TFSI and [Li-G4]TFSI, respectively. Reactants were stirred at room temperature for two days and subsequently dried under high vacuum for 1 h at 140 °C to remove residual water. Water content, measured by Karl Fischer titration, is detailed in ESI table S2.

Table 1 Investigated SIL samples showing the sample name & composition, lithium to ether ratio, ether oxygen atom to lithium ratio & ether oxygen atom per 4 oxygen atoms to lithium ratio.

Ether:LiTFSI	$r = \frac{[Li]}{[ETH]}$	$r_{EO} = \frac{No.ETH\ O}{Li}$	$r_{4EO} = \frac{No.4\ ETH\ O}{Li}$
G3-1:1	1.0	4.00	1.00
G3-1:1.5	1.5	2.67	0.67
G3-1:2	2.0	2.00	0.50
G3-1:2.5	2.5	1.60	0.40
G3-1:3	3.0	1.33	0.33
G3-1:3.5	3.5	1.14	0.29
G3-1:4	4.0	1.00	0.25
G4-1:1	1.0	5.00	1.25
G4-1:1.25	1.25	4.00	1.00
G4-1:1.5	1.5	3.33	0.83
G4-1:1.75	1.75	2.86	0.71
G4-1:2	2.0	2.50	0.63
G4-1:2.5	2.5	2.00	0.50
G4-1:3	3.0	1.67	0.42

In the table *r* is the molar ratio of LiTFSI to glyme. r_{EO} is the number of ether oxygen atoms present in G3 or G4 per lithium atom. r_{4EO} is the ratio of ether oxygen atoms to lithium atoms per 4 ether oxygen atoms, derived from template synthesis of 12-Crown-4 ethers, lithium is the favoured group 1 cation for 12-Crown-4 ethers.[32]

Results and Discussion

Diffusion NMR

Fitting of relaxation data, for ^{7}Li, ^{1}H and ^{19}F nuclei, did not indicate the existence of more than one diffusing nuclei population per nuclei in each SIL sample. However, PFG-NMR measurements capture averaged diffusing species in SIL samples, so Li^+ transference numbers (t_{Li}) calculated from PFG-NMR data include transport of both associated and dissociated species (if any). The data showed decreasing diffusion speeds of nuclei with increasing LiTFSI concentration and decreasing temperature (**Fig. 2a** & **2b**). This is unsurprising and consistent with the temperature dependence viscosity of SIL samples (**Fig. 3** & **Fig. 3**).

The t_{Li} for G3-1:1 and G4-1:1, 0.61 and 0.52, respectively, and diffusion coefficients D_{Li} 0.89, D_H 0.84 & D_F 0.57 for G3 and D_{Li} 1.31, D_H 1.29 & D_F 1.22 for G4 (all x10^{-7} cm^2s^{-1}) reported by Yoshida *et al*. 2011 at 30 °C indicated Li^+, $TFSI^-$ & Glyme all diffuse at approximately the same speeds in the SILs. Diffusion coefficients differed by a maximum of 0.09 of an order of magnitude with the exception of G3 F, differing by just under 1/3rd of an order of magnitude from G3 Li.[20] All t_{Li} calculated from PFG-NMR data are detailed in table S3 & S4 (ESI).

Notably, t_{Li} for G3-1:1 at 70-80 °C (t_{Li} = 0.71, 0.75 & 0.80, respectively) and G3-1:1.5 at 80 °C (t_{Li} = 0.67) indicate Li^+ is diffusing significantly faster than the TFSI counter anion. Statistically significant faster Li^+ diffusion than the glyme (G3) and TFSI in G3-1:1 at 70-80 °C & G3-1:1.5 at 80 °C is shown in **Fig. 2a**, where an increasing deviation in t_{Li} is noted compared to the fluorine. In the G4 system, significantly faster lithium diffusion, relative to glyme and anion, was observed for G4-1:1 for 5 °C increments between 65-80 °C (t_{Li} = 0.64. 0.69, 0.75, 0.80, respectively) and G4-1:1.25 at 75-80 °C (t_{Li} = 0.65 & 0.72, respectively). Furthermore, Li^+ diffusing significantly faster than other species, albeit by a smaller margin, was observed in G4-1:1.25 at 75-80 °C, G4-1:1.5 at 80 °C & G4-1:2 at 75-80 °C (**Fig. 2b**).

The exact mechanism of this difference in diffusion is unknown but it is possible that, at higher temperatures, Li^+ may have sufficient energy to dissociate from the ligand coordination with G3 or G4 and participate in a hopping effect, jumping from ligand to ligand. The G3 ligand, with 4 ether oxygens, is the ideal binding size for the Li^+ cation. Whereas, G4 with 5 ether oxygens, is larger and has a looser chelation with the Li^+ cation. This is supported by longer Li^+-O bond lengths being reported for G4, suggesting a weaker interaction between the Li^+ cation and the ligand, relative to G3.[51] Similarly, molecular dynamics simulation (vide infra) shows that G4-1:1 has a lower interaction with sulfonamide oxygen (i.e. Li-O(TFSI)) than both the G4-1:1.25 and G3-1:1, supporting the proposed extra chelation ability of G4. This mechanism is explored in greater detail below.

Nevertheless, our observations are consistent with PFG-NMR findings here showing Li^+ diffuses faster than other species in the G4-derived SIL at lower temperatures than when the G3 ligand is used. **Fig. 2c** shows Li^+ diffusing statistically significantly faster in G4 samples than the analogous G3 samples between the ratios of 1:1 and 1:2.

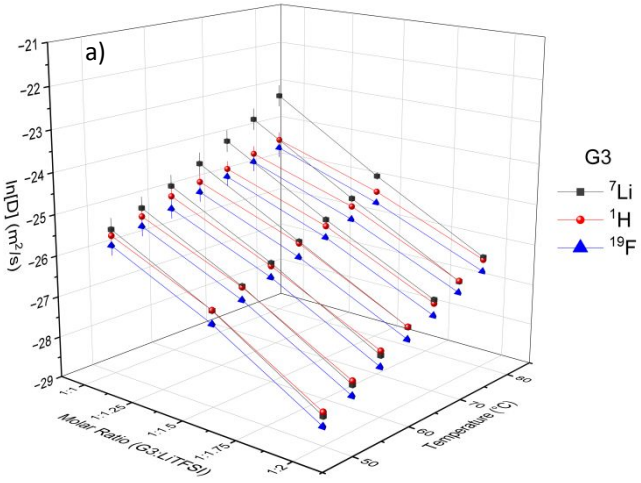

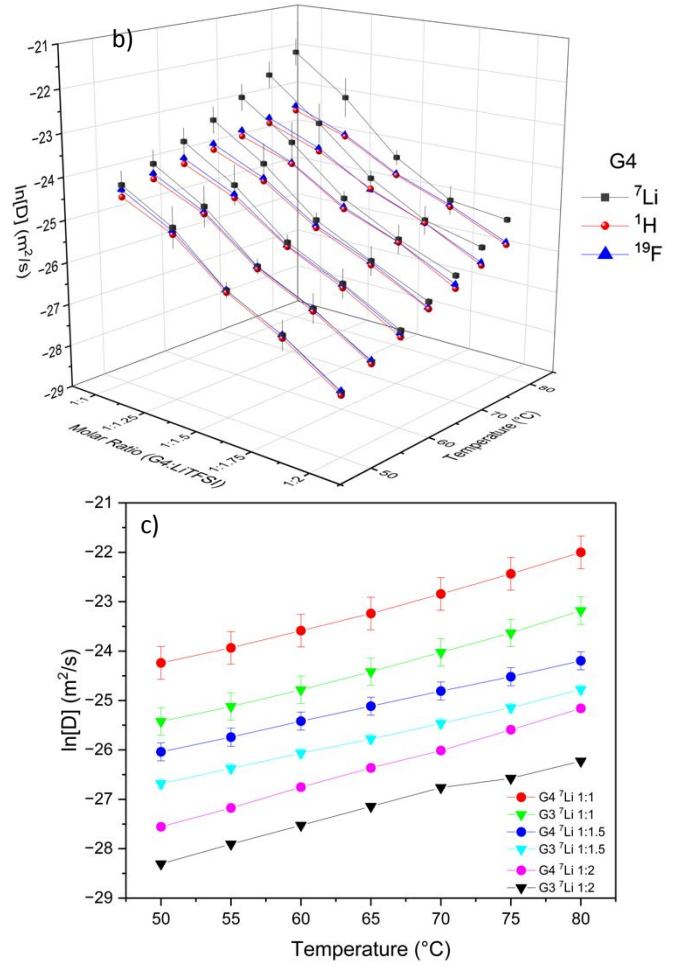

Fig. 2 (a) A 3D plot showing Ln of diffusion coefficients of ^{7}Li, ^{1}H and ^{19}F nuclei present in Li, glyme & TFSI components of SIL samples G3-1:1 through to G3-1:2 across the 50-80 °C temperature range. (b) A 3D plot showing 50-80 °C diffusion data for G4-1:1 through to G4-1:2 SIL samples. (c) A 2D plot showing Li nuclei 50-80 °C diffusion data for G3 and G4 samples 1:1 through to 1:2. Figures S5-S7 plot these plots (a-c) without connecting lines to avoid misleading false cusps.

At lower temperatures (20-60 °C) the PFG-NMR results were consistent with previous findings where all three SIL components diffuse at approximately the same speeds (**Fig. 2a**, **Fig. 2b**, S1, S2, S8 & S9). Higher concentration SILs showed the expected continued reduction in diffusion speeds as LiTFSI concentration was increased (S3, S4, S10 & S11), likely due to viscosity increases.

Thermal properties

Temperature dependence of SIL sample viscosity was measured by rheology. SIL samples displayed rapid reduction in viscosity with temperature increase (**Fig. 3**). G3 samples had higher viscosity at each LiTFSI ratio than G4 samples (**Fig. 3** & S12-S16), as would be expected considering the coordinative capability of the G3 glyme. Viscosity measurements with VFT fitting curves are shown in figures S12-S16 (ESI). The temperature-dependent viscosity reduction of G3 & G4 SILs makes them suitable for use in manufacturing processes. Raising the temperature, for example, to 50-60 °C, will exponentially lower the viscosity of high Li^+ concentration SILs, enabling their processing as thin liquids that solidify or gel upon cooling. This provides a means for the electrolyte to 'wet out' the electrodes, separator, etc. efficiently, before cooling to a gel and thus retaining their desirable spill mitigation properties. Viscosity best-fit parameters are summarised in table S11.

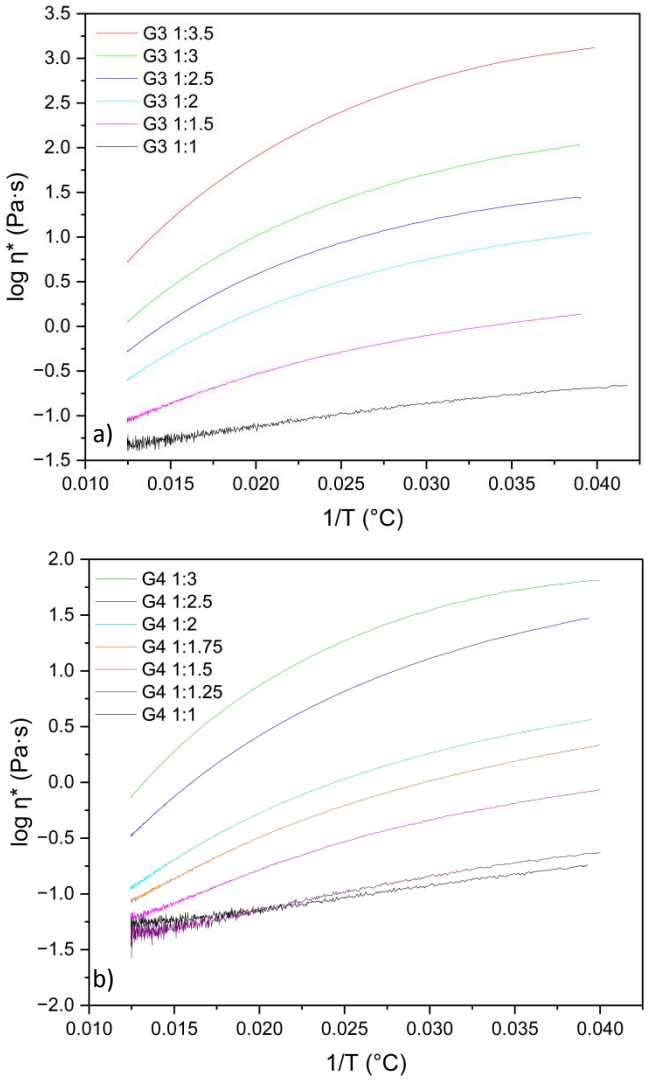

Fig. 3 Log_{10} complex viscosity vs 1/temperature for (a) G3 and (b) G4 SIL samples.

Thermal stabilities

Thermogravimetric mass loss curves (**Fig. 4a** & **Fig. 4b**) display multistep mass losses for SIL samples. The temperature at which a 5% mass loss occurred for SIL samples, T_d (°C), increases with increasing LiTFSI concentration (**Fig. 4c**). The T_d for neat G3 and G4 is 103 °C and 133 °C, respectively.[43] In 1:1 SIL ratios when the Li cation coordinates with oligo-ethers (G3 or G4) the T_d of the resulting SIL is raised to 212.1 °C and 204.5 °C for G3-1:1 and G4-1:1, respectively (**Fig. 4**). Raman spectroscopy of G3-1:1 and G4-1:1 showed free G3 and G4 in these SILs was a negligible percentage,[51] however a population of free G3 and G4 still exists in 1:1 ratios. Aguilera *et al.* found through Raman spectroscopy fitting a population of $TFSI^-$ coordinated with Li^+ existed in G4:LiTFSI at equimolar ratios, and hence concluded a population of uncoordinated G4 was also present at equimolar ratios.[44] As LiTFSI concentration increases this would,

theoretically, increase the amount of Li^+ available to coordinate with 'uncoordinated' glyme oxygen species and hence push the equilibrium ratio of free-glyme:coordinated-glyme towards the latter. This would correlate to a reduced population of free glyme at higher Li^+ concentrations, thereby increasing the T_d of the SIL. The T_d of G4 SILs upwards from G4-1:1.5 in concentration is likely dominated not by ether Li^+ coordination, as the G4 T_d of these samples is higher than G3 which coordinates the Li^+ more strongly but by increased carbon chain length and molecular weight, as is the case for pure G4 vs. G3 T_d. T_d of G4-1:1.5 upwards is also possibly influenced by the increased coordination of multiple Li^+ cations by a single G4 ligand, which occurs more so for G4 than G3 due to G4's longer ethereal chain length. Notably, the T_d of all SIL samples exceeds that of organic solvents typically used in traditional LIBs (e.g. carbonate solvents, ethylene carbonate, etc.) and further illustrates their suitability as thermally stable and safe electrolytes in LIBs and supercapacitors.[9] Isothermal stability of SIL samples was not performed as Yoshida *et al*. has previously reported the isothermal thermal mass loss of G3/G4:LiTFSI at equimolar ratios. The observed SIL T_d trend would likely be replicated in isothermal stability.[20]

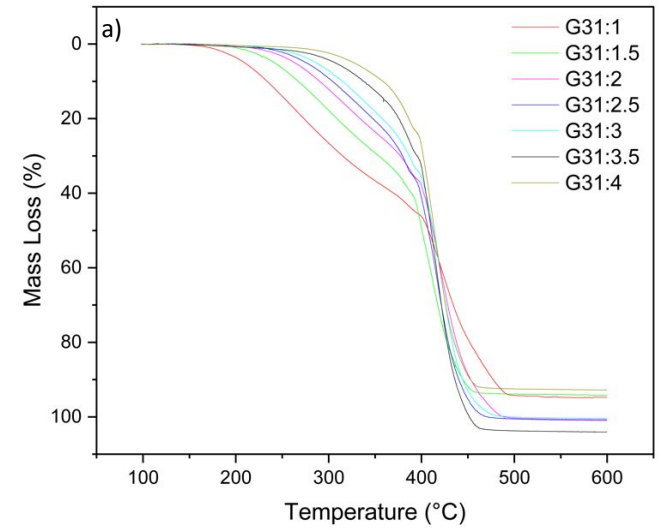

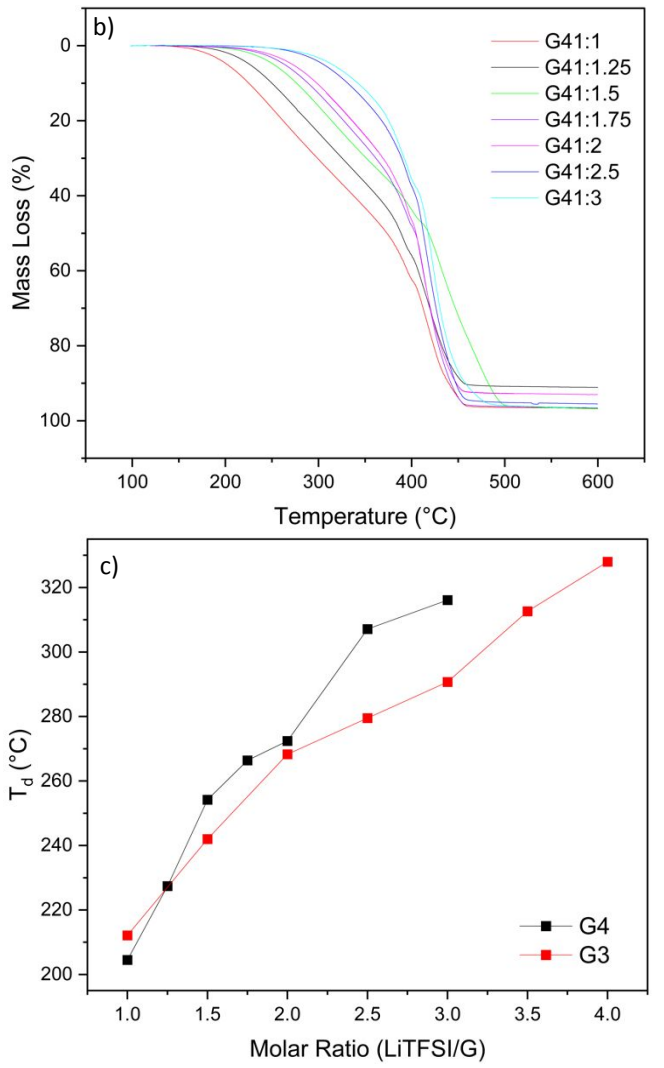

Fig. 4 (a)TG curves for G3 samples. (b) TG curves for G4 samples. (c) A plot showing T_d °C for G3 and G4 samples. Reported T_d °C are detailed in Table S14 (ESI). Figure S19 plots 4c without connecting lines to avoid misleading false cusps.

Assuming that T_d is an indication of 'uncoordinated glyme', then G4-1:1 possessing a T_d lower than G3-1:1 T_d (**Fig. 4c**) would indicate greater coordination between Li^+ and G3 at 1:1 ratio than G4. This is consistent with G4-1:1 having too many ether oxygens (5) per Li^+ for optimum binding at a 1:1 ratio. The T_d for G4-1:1.25, oxygen:lithium ratio of 4:1, adds further credence to this hypothesis as it is higher than the G3-1:1 T_d.

DSC thermograms for G3&G4-1:1 through to 1:2 SIL samples are shown in figures S17 & S18 (ESI). The G4-1:1 possessed a glass transition temperature (T_g) of -54.0 °C and G3-1:1 T_m of 20.7 °C correlate to T_g and T_m of -54 °C and 23 °C, respectively, reported in literature.[12, 30, 43] A pattern of increasing glass transition temperature (T_g) and increasing RT liquid-liquid phase transition temperature (T_l/$_L$) is evident in G4 samples with increasing LiTFSI concentration. DSC measurements were performed repeatedly on SIL samples, with reproducible results.

Ion dynamic properties

Ionic conductivity, ion mobility under an electrical potential, was assessed in G3&G4-1:1, at 0.25 (G4) and 0.5 (G3) molar increments, from 1:1 to 1:2 (glyme: LiTFSI) SIL samples using electrochemical impedance spectroscopy (EIS). Ionic conductivity, displayed in **Fig. 5**, shows a decreasing trend with increasing LiTFSI concentration. G4 SIL samples show 10.65%, 29.52% and 78.14% higher ionic conductivity than G3 at 1:1, 1:1.5 and 1:2 ratios, respectively. Through line of best fit extrapolation (table S18), the same ionic conductivity of G3-1:1 can be achieved by a G4 ratio of G4-1:1.19.

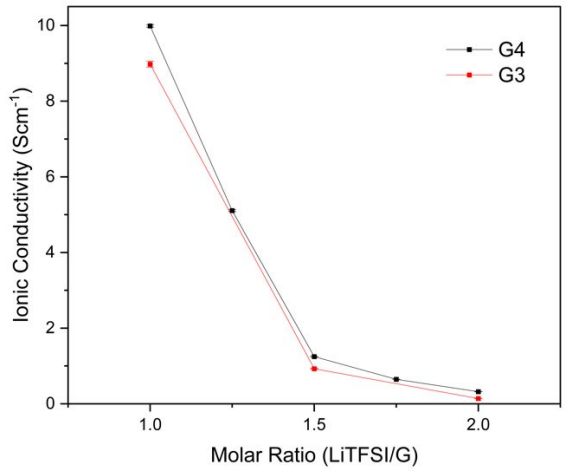

Fig. 5 Ionic conductivity values with standard error for G3&G4-1:1 through to 1:2 SIL samples. Reported values and raw data are detailed in Table S15-17 (ESI). Figure S20 plots fig. 5 without connecting lines to avoid misleading false cusps.

Molecular Dynamics Simulations

Classical molecular dynamics simulations were conducted for the G3-1:1, G4-1:1 and G4-1:1.25 systems to explore the possible mechanism of lithium diffusion at higher temperatures. Radial distribution functions (RDFs) and coordination number distributions of lithium to O(TFSI), O(G3) and O(G4) are shown in Fig. S10 and S11. These indicate that although all the glyme-Li^+ interactions are approximately equal between G3-1:1, G4-1:1 and G4-1:1.25, the $TFSI^-$ interaction with Li^+ is weaker in G4-1:1 compared with G3-1:1 and G4-1:1.25.

The simulations were also able to estimate the proportion of free (un-coordinated) glyme in the liquids at room temperature. The amount of free glyme is negligible (2.3%) for G3-1:1, 2.6% for G4-1:1 and 1.5% for G4-1:1.25. These values correspond well with the proportion of free G4 inferred from fits based on neutron diffraction[52] and Raman spectroscopy. Additionally, these support the hypothesis outlined above based on T_d where G3-1:1 has a higher T_d than G4-1:1 due to a slightly higher amount of free glyme, and that the G4-1:1.25 sample has a lower proportion of free glyme resulting in a higher T_d.

Simulations were conducted at a substantially elevated temperatures of 227 °C (where lithium enters a "diffusive regime" using the force field) and 427 °C and were unable recover the observed trend of markedly increased diffusion of lithium relative to the other components of the liquid (Table S19). However, it is noted that simulations reported by Dong and Bedrov, based on polarisable force fields, have also been unable to recover this behaviour, with the authors ultimately concluding that lithium diffuses with a segmental motion in its solvation sphere.[53]

Nonetheless, the current simulations at 427 °C revealed lithium diffusion *via* a "hopping" mechanism with the glyme molecules facilitating this hopping by bridging between two lithium ions, as indicated by complexes **(4)** and **(5)** in **Fig. 6a**. This mechanism was observed several times within each of the production run trajectories at the elevated temperature of 427 °C. Fig 6a summarises one such event. The mechanism begins with the G4 molecules increasingly converting to mono/bi/tridentate coordination with the lithium at the higher temperature in contrast with their coordination *via* all five of their oxygens at 25 °C (**Fig. 6b**). The free $TFSI^-$ ions make up the rest of the first coordination sphere, until a G4-Li solvate complex interacts with an all TFSI-coordinated Li^+. This leads to the formation of a Li-G4-Li bridging complex that eventually loses one lithium and becomes a new Li-G4 solvate complex (complex **(6)** in **Fig. 6a**). Although there is an average increase in the proportion of $TFSI^-$ coordinating to Li^+ in the G4-1:1, there is no change to $TFSI^-$ coordination structure in the G4-1:1.25 (shown in Fig. S12). The role of the $TFSI^-$ anions is therefore significant in this lithium hopping mechanism as the latter ratio has a slightly lower diffusion coefficient. Although this type of hopping mechanism has been previously hypothesised in the literature,[54] no direct evidence to support this has been reported to date. Simulations at elevated temperatures of 227 °C and 427 °C do not represent the real system at 30 °C and 80 °C but provide supportive evidence of a likely mechanism hypothesised by experiment. Previous reports using this force field and scaled charges also used elevated temperatures of 227 °C to discern diffusion coefficient trends and conduction mechanisms. More efforts in this area are required to recover the diffusion trends observed within this current work which are challenging for other previous work as well.[55-57]

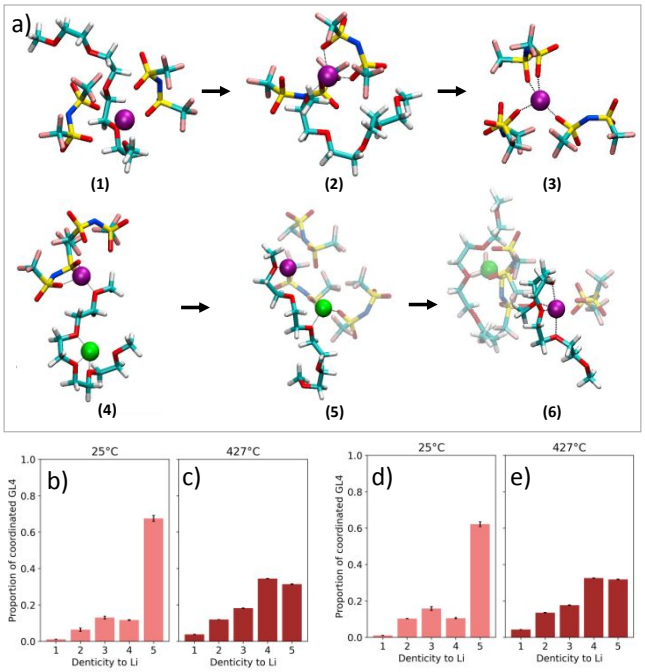

Fig. 6 (a) Example of the hopping mechanism of lithium diffusion taken from simulations at 427 °C of GL4-1:1 and GL4-1:1.25. The pink atom is the lithium followed throughout the trajectory. The green atom is a lithium that is complexed to a new GL4 molecule. (b) and (c) Histograms of the proportion of GL4 and their respective denticity to a lithium ion in GL4-1:1 at 25 °C and at 427 °C. (d) and (e) Histograms of the proportion of GL4 and their respective denticity to a lithium ion in GL4-1:1.25 at 25 °C and at 427 °C.

Conclusions

Self-diffusion properties of G3/G4:LiTFSI were found to be temperature and Li^+ concentration/viscosity dependant. Li^+ acceleration, characterised by the independent and faster movement of Li^+ compared to glyme and anion components, was observed in G3-1:1 (70-80 °C), G4-1:1 (65-80 °C), G3-1:1.5 and G4-1:1.5 (80 °C), and G4-1:1.25 and G4-1:2 (75-80 °C). Molecular dynamics simulation supports the proposed mechanism of lithium 'hopping' between glyme units facilitated by the TFSI anion.

The viscosity of SIL samples was found to exhibit temperature-dependent exponential thermal thinning behaviour, indicating the suitability of SILs for thermal infusion manufacturing processes. The thermal stability of SIL samples was confirmed, and higher LiTFSI concentration samples were shown to be stable electrolytes with T_d °C values exceeding those of traditional LIB organic solvents. These properties make them suitable for use in LIBs and structural supercapacitors. The G4-1:1 T_d °C value being less than the G3-1:1 T_d °C, despite pure G4 having a T_d °C 30 °C higher than pure G3 confirmed 4-ether oxygens per Li atom as the ideal chelating ratio. These findings suggest ether oxygen:cation ratio should be used to define ethereal SILs component ratios instead of stoichiometric ratios outlined in SIL criteria by Mandai *et al*.[29]

Ionic conductivity findings showed G4 SIL 1:1 to 1:2 ratios had >10% higher ionic conductivity than comparable G3 ratios. These findings have practical implications for future research on structural CF supercapacitors, such as those reported by Dharmasiri *et al*.,[19] to increase the energy storage performance of these devices. The comparatively higher ionic conductivity of G4 than G3 means that G4-1:1.19 can be used as a substitute to G3-1:1 with the same ionic conductivity, in the same volume, but with more Li^+ cations present to store charge.

Planned future work on SIL optimisation involves investigating higher lithium concentrations using tetraglyme-monoethyl:LiTFSI, reported as [Li(G4Et)][TFSA] by Tamura *et al*. to have desirable properties, including 27% lower viscosity, 2% lower density, 23% higher Li^+ self-diffusion speed, and similar ionic conductivity and t_{Li} as G4-1:1.[12] These properties make tetraglyme-monoethyl:LiTFSI ideal for investigation as a SIL solvent for lithium 'packing' in higher lithium concentration SILs.

Author Contributions

Timothy Harte: data curation, formal analysis, investigation, methodology, validation, visualisation, conceptualisation, writing – original draft, writing – review & editing. Bhagya Dharmasiri: methodology, conceptualisation, project administration, supervision, review & editing. Luke C. Henderson: methodology, conceptualisation, project administration, funding acquisition, supervision, resources, review & editing. Garima S. Dobhal: computational data curation and analysis, visualisation, writing – Molecular Dynamics simulations section. Tiffany R. Walsh: methodology, conceptualisation, supervision, funding acquisition, resources, editing & review.

Conflicts of interest

There are no conflicts to declare.

Acknowledgements

The authors would like to express their gratitude to Deakin University and the Australian Research Council (ARC) Discovery Programme (DP220100130), as well as the ARC Linkage Infrastructure, Equipment, and Facilities (LIEF) grant (LE110100141) for supporting the Deakin University Magnetic Resonance Facility. This work was also made possible by the support of the Office of Naval Research Global (N62909-22-1-2052). This research was conducted at the Deakin University Institute for Frontier Materials and Carbon Nexus facilities. The authors thank Deakin NMR and technical staff, in particular I. E. Gunathilaka for training TH on diffusion NMR techniques. The theoretical work for this project was undertaken with the assistance of resources and services from the National Computational Infrastructure (NCI), which is supported by the Australian Government.

ARTICLE

References

1. D. J. Eyckens, M. E. Champion, B. L. Fox, P. Yoganantharajah, Y. Gibert, T. Welton and L. C. Henderson, Solvate ionic liquids as reaction media for electrocyclic transformations. *Eur. J. Org. Chem.*, 2016.
2. M. Armand, F. Endres, D. R. MacFarlane, H. Ohno and B. Scrosati, Ionic-liquid materials for the electrochemical challenges of the future, *Nat. Mater.*, 2009, **8**, 621-629.
3. N. V. Plechkova and K. R. Seddon, Applications of ionic liquids in the chemical industry, *Chem. Soc. Rev.*, 2008, **37**, 123-150.
4. K. S. Egorova, E. G. Gordeev and V. P. Ananikov, Biological activity of ionic liquids and their application in pharmaceutics and medicine, *Chem. Rev.*, 2017, **117**, 7132-7189.
5. M. A. P. Martins, C. P. Frizzo, A. Z. Tier, D. N. Moreira, N. Zanatta and H. G. Bonacorso, Update 1 of: Ionic Liquids in Heterocyclic Synthesis, *Chem. Rev.*, 2014, **114**, PR1-PR70.
6. H. Weingärtner, Understanding ionic liquids at the molecular level: facts, problems, and controversies, *Angew. Chem. Int. Ed.*, 2008, **47**, 654-670.
7. A. Lewandowski and A. Świderska-Mocek, Ionic liquids as electrolytes for Li-ion batteries—An overview of electrochemical studies, *J. Power Sources*, 2009, **194**, 601-609.
8. A. Balducci, Ionic liquids in lithium-ion batteries, *Ionic Liquids II*, 2018, 1-27.
9. K. Xu, Nonaqueous liquid electrolytes for lithium-based rechargeable batteries, *Chem. Rev.*, 2004, **104**, 4303-4418.
10. M. Lu, X. Zhang, J. Ji, X. Xu and Y. Zhang, Research progress on power battery cooling technology for electric vehicles, *J. Energy Storage*, 2020, **27**, 101155.
11. C. A. Angell, Y. Ansari and Z. Zhao, Ionic liquids: past, present and future, *Faraday discussions*, 2012, **154**, 9-27.
12. T. Tamura, K. Yoshida, T. Hachida, M. Tsuchiya, M. Nakamura, Y. Kazue, N. Tachikawa, K. Dokko and M. Watanabe, Physicochemical properties of glyme–Li salt complexes as a new family of room-temperature ionic liquids, *Chem. Lett*, 2010, **39**, 753-755.
13. T. Kawazoe, K. Hashimoto, Y. Kitazawa, H. Kokubo and M. Watanabe, A Polymer electrolyte containing solvate ionic liquid with increased mechanical strength formed by self-assembly of ABA-type ionomer triblock copolymer, *Electrochim. Acta*, 2017, **235**, 287-294.
14. R. Kido, K. Ueno, K. Iwata, Y. Kitazawa, S. Imaizumi, T. Mandai, K. Dokko and M. Watanabe, Li+ ion transport in polymer electrolytes based on a glyme-Li salt solvate ionic liquid, *Electrochim. Acta*, 2015, **175**, 5-12.
15. T. Nakazawa, A. Ikoma, R. Kido, K. Ueno, K. Dokko and M. Watanabe, Effects of compatibility of polymer binders with solvate ionic liquid electrolytes on discharge and charge reactions of lithium-sulfur batteries, *J. Power Sources*, 2016, **307**, 746-752.
16. K. Ueno, J.-W. Park, A. Yamazaki, T. Mandai, N. Tachikawa, K. Dokko and M. Watanabe, Anionic effects on solvate ionic liquid electrolytes in rechargeable lithium–sulfur batteries, *J. Phy. Chem. C*, 2013, **117**, 20509-20516.
17. D. J. Eyckens, L. Servinis, C. Scheffler, E. Wölfel, B. Demir, T. R. Walsh and L. C. Henderson, Synergistic interfacial effects of ionic liquids as sizing agents and surface modified carbon fibers, *J. Mater. Chem. A*, 2018, **6**, 4504-4514.
18. D. J. Eyckens and L. C. Henderson, Synthesis of α-aminophosphonates using solvate ionic liquids, *RSC Adv.*, 2017, **7**, 27900-27904.
19. B. Dharmasiri, F. Stojcevski, K. A. S. Usman, S. A. Qin, J. M. Razal, E. H. Doeven, P. S. Francis, T. U. Connell, Y. Yin and G. G. Andersson, Flexible carbon fiber based structural supercapacitor composites with solvate ionic liquid-epoxy solid electrolyte, *Chem. Eng. J.*, 2023, **455**, 140778.
20. K. Yoshida, M. Tsuchiya, N. Tachikawa, K. Dokko and M. Watanabe, Change from glyme solutions to quasi-ionic liquids for binary mixtures consisting of lithium bis (trifluoromethanesulfonyl) amide and glymes, *J. Phy. Chem. C*, 2011, **115**, 18384-18394.
21. E. W. Castner Jr, J. F. Wishart and H. Shirota, Intermolecular dynamics, interactions, and solvation in ionic liquids, *Acc. Chem. Res.*, 2007, **40**, 1217-1227.
22. T. Welton, Ionic liquids: a brief history, *Biophys. Rev.*, 2018, **10**, 691-706.
23. O. E. Bankole, C. Gong and L. Lei, Battery recycling technologies: Recycling waste lithium ion batteries with the impact on the environment in-view, *J. Environ. Ecol*, 2013, **4**, 14-28.
24. P. Yoganantharajah, D. J. Eyckens, J. L. Pedrina, L. C. Henderson and Y. Gibert, A study on acute toxicity and solvent capacity of solvate ionic liquids in vivo using a zebrafish model (Danio rerio), *New J. Chem.*, 2016, **40**, 6599-6603.
25. R. Mahakali, F. Kuipers, A. Yan, W. Anderson and T. Pourpoint, Development of reduced toxicity hypergolic propellants, *47th AIAA/ASME/SAE/ASEE Joint Propulsion Conference & Exhibit*, 2011.
26. W. A. Henderson, N. R. Brooks and V. G. Young, Tetraglyme− Li+ cation solvate structures: models for amorphous concentrated liquid and polymer electrolytes (II), *Chem. Mater.*, 2003, **15**, 4685-4690.
27. W. A. Henderson, N. R. Brooks, W. W. Brennessel and V. G. Young, Triglyme− Li+ cation solvate structures: models for amorphous concentrated liquid and polymer electrolytes (I), *Chem. Mater.*, 2003, **15**, 4679-4684.
28. J. Tong, S. Wu, N. Von Solms, X. Liang, F. Huo, Q. Zhou, H. He and S. Zhang, The effect of concentration of lithium

salt on the structural and transport properties of ionic liquid-based electrolytes, *Front. Chem.*, 2020, **7**, 945.
29. T. Mandai, K. Yoshida, K. Ueno, K. Dokko and M. Watanabe, Criteria for solvate ionic liquids, *Phys. Chem. Chem. Phys.*, 2014, **16**, 8761-8772.
30. D. J. Eyckens and L. C. Henderson, A review of solvate ionic liquids: Physical parameters and synthetic applications, *Front. Chem.*, 2019, **7**, 263.
31. Z. Wan, H. Lu, J. Yang, Y. Zhang, F. Lin, J. Xia, X. Yao, J. Luo and C. Jia, Chelation of lithium ion with crown ether for eliminating adverse effects caused by Li-TFSI/tBP doping system in Spiro-OMeTAD, *J. Energy Chem.*, 2022, **74**, 489-496.
32. B. R. Bowsher and A. J. Rest, Use of alkali- and alkaline-earth-metal ions in the template synthesis of 12-crown-4, 15-crown-5, and 18-crown-6, *J. Chem. Soc, Dalton Trans.*, 1981, DOI: 10.1039/DT9810001157, 1157-1161.
33. K. Dokko, N. Tachikawa, K. Yamauchi, M. Tsuchiya, A. Yamazaki, E. Takashima, J.-W. Park, K. Ueno, S. Seki and N. Serizawa, Solvate ionic liquid electrolyte for Li–S batteries, *J. Electrochem. Soc.*, 2013, **160**, A1304.
34. Y. Yuan, X. Peng, B. Wang, K. Xue, Z. Li, Y. Ma, B. Zheng, Y. Song and H. Lu, Solvate ionic liquid-derived solid polymer electrolyte with lithium bis (oxalato) borate as a functional additive for solid-state lithium metal batteries, *J. Mater. Chem. A*, 2023.
35. L. Zeng, T. Wu, T. Ye, T. Mo, R. Qiao and G. Feng, Modeling galvanostatic charge–discharge of nanoporous supercapacitors, *Nat. Comput. Sci.*, 2021, **1**, 725-731.
36. D. Bedrov, J.-P. Piquemal, O. Borodin, A. D. MacKerell Jr, B. Roux and C. Schröder, Molecular dynamics simulations of ionic liquids and electrolytes using polarizable force fields, *Chem. Rev.*, 2019, **119**, 7940-7995.
37. M. Z. Bazant, B. D. Storey and A. A. Kornyshev, Double layer in ionic liquids: Overscreening versus crowding, *Phys. Rev. Lett.*, 2011, **106**, 046102.
38. M. V. Fedorov and A. A. Kornyshev, Ionic liquids at electrified interfaces, *Chem. Rev.*, 2014, **114**, 2978-3036.
39. B. Shen, R. Guo, J. Lang, L. Liu, L. Liu and X. Yan, A high-temperature flexible supercapacitor based on pseudocapacitive behavior of FeOOH in an ionic liquid electrolyte, *J. Mater. Chem. A*, 2016, **4**, 8316-8327.
40. M. C. R. B. Madden and P.-L. S. P. Taberna, Gogotsi Y. Salanne M. On the molecular origin of supercapacitance in nanoporous caaarbon electrodes, *Nat Mater*, 2012, **11**, 306-310.
41. C. Merlet, C. Péan, B. Rotenberg, P. A. Madden, B. Daffos, P.-L. Taberna, P. Simon and M. Salanne, Highly confined ions store charge more efficiently in supercapacitors, *Nat. Commun.*, 2013, **4**, 2701.
42. A. C. Forse, C. Merlet, J. M. Griffin and C. P. Grey, New perspectives on the charging mechanisms of supercapacitors, *J. Am. Chem. Soc.*, 2016, **138**, 5731-5744.
43. K. Ueno, K. Yoshida, M. Tsuchiya, N. Tachikawa, K. Dokko and M. Watanabe, Glyme–lithium salt equimolar molten mixtures: concentrated solutions or solvate ionic liquids?, *J. Phys. Chem. B*, 2012, **116**, 11323-11331.
44. L. Aguilera, S. Xiong, J. Scheers and A. Matic, A structural study of LiTFSI–tetraglyme mixtures: From diluted solutions to solvated ionic liquids, *J. Mol. Liq.*, 2015, **210**, 238-242.
45. P. Jankowski, M. Dranka, W. Wieczorek and P. Johansson, TFSI and TDI anions: Probes for solvate ionic liquid and disproportionation-based lithium battery electrolytes, *J. Phys. Chem. Lett.*, 2017, **8**, 3678-3682.
46. I. E. Gunathilaka, A. Taheri, J. M. Pringle, M. Forsyth and L. A. O'Dell, Probing the molecular interactions and physicochemical properties of a cobalt-based redox electrolyte system for thermo-electrochemical cells, *Phys. Chem. Chem. Phys.*, 2022, **24**, 27772-27782.
47. K. Shigenobu, K. Dokko, M. Watanabe and K. Ueno, Solvent effects on Li ion transference number and dynamic ion correlations in glyme-and sulfolane-based molten Li salt solvates, *Phys. Chem. Chem. Phys.*, 2020, **22**, 15214-15221.
48. Q. Zheng and J. C. Mauro, Viscosity of glass-forming systems, *J. Am. Ceram. Soc.*, 2017, **100**, 6-25.
49. N. Hameed, D. J. Eyckens, B. M. Long, N. V. Salim, J. C. Capricho, L. Servinis, M. De Souza, M. D. Perus, R. J. Varley and L. C. Henderson, Rapid Cross-Linking of Epoxy Thermosets Induced by Solvate Ionic Liquids, *ACS Appl. Polym. Mater.*, 2020, **2**, 2651-2657.
50. S. P. Li, G. Zhao and H. Y. Chen, The relationship between steady shear viscosity and complex viscosity, *J. Disper. Sci. Technol.*, 2005, **26**, 415-419.
51. K. Ueno, R. Tatara, S. Tsuzuki, S. Saito, H. Doi, K. Yoshida, T. Mandai, M. Matsugami, Y. Umebayashi and K. Dokko, Li+ solvation in glyme–Li salt solvate ionic liquids, *Phys. Chem. Chem. Phys.*, 2015, **17**, 8248-8257.
52. T. Murphy, S. K. Callear, N. Yepuri, K. Shimizu, M. Watanabe, J. N. C. Lopes, T. Darwish, G. G. Warr and R. Atkin, Bulk nanostructure of the prototypical 'good'and 'poor'solvate ionic liquids [Li (G4)][TFSI] and [Li (G4)][NO 3], *Phys. Chem. Chem. Phys.*, 2016, **18**, 17224-17236.
53. D. Dong and D. Bedrov, Charge transport in [Li (tetraglyme)][bis (trifluoromethane) sulfonimide] solvate ionic liquids: insight from molecular dynamics simulations, *J. Phys. Chem. B*, 2018, **122**, 9994-10004.
54. A. Kitada, Y. Koujin, M. Shimizu, K. Kawata, C. Yoshinaka, M. Saimura, T. Nagata, M. Katahira, K. Fukami and K. Murase, Glyme-Lithium Bis (trifluoromethylsulfonyl) amide Super-concentrated Electrolytes: Salt Addition to Solvate Ionic Liquids Lowers Ionicity but Liberates Lithium Ions, *J. Electrochem. Soc.*, 2021, **168**, 090521.
55. A. Thum, A. Heuer, K. Shimizu and J. N. C. Lopes, Solvate ionic liquids based on lithium bis (trifluoromethanesulfonyl) imide–glyme systems: Coordination in MD simulations with scaled charges, *Phys. Chem. Chem. Phys.*, 2020, **22**, 525-535.
56. S. Tsuzuki, W. Shinoda, M. Matsugami, Y. Umebayashi, K. Ueno, T. Mandai, S. Seki, K. Dokko and M. Watanabe, Structures of [Li (glyme)]+ complexes and their interactions with anions in equimolar mixtures of glymes and Li [TFSA]: analysis by molecular dynamics simulations, *Phys. Chem. Chem. Phys.*, 2015, **17**, 126-129.
57. W. Shinoda, Y. Hatanaka, M. Hirakawa, S. Okazaki, S. Tsuzuki, K. Ueno and M. Watanabe, Molecular dynamics study of thermodynamic stability and dynamics of [Li (glyme)]+ complex in lithium-glyme solvate ionic liquids, *Chem. Phys.*, 2018, **148**.